ACS APPLIED MATERIALS & INTERFACES

Research Article

www.acsami.org

Organic Dyes Containing Carbazole as Donor and π-Linker: Optical, Electrochemical, and Photovoltaic Properties

A. Venkateswararao,[†] K. R. Justin Thomas,*[,†] Chuan-Pei Lee,[‡] Chun-Ting Li,[‡] and Kuo-Chuan Ho[‡]

[†]Organic Materials Laboratory, Department of Chemistry, Indian Institute of Technology Roorkee, Roorkee-247 667, India

[‡]Department of Chemical Engineering, National Taiwan University, Taipei 10617, Taiwan.

Supporting Information

ABSTRACT: A series of new metal free organic dyes containing carbazole as donor and π-linker have been synthesized and characterized as effective sensitizers for dye sensitized solar cells (DSSCs). The carbazole functionalized at C-2 and C-7 served as electron-rich bridge. The donor property of the carbazole is substantially enhanced on introduction of *tert*-butyl groups at C-3 and C-6 positions and the oxidation propensity of the dyes increased on insertion of thiophene unit in the conjugation pathway. These structural modifications fine-tuned the optical and electrochemical properties of the dyes. Additionally, the presence of *tert*-butyl groups on the carbazole nucleus minimized the intermolecular interactions which benefited the performance of DSSCs. The dyes served as efficient sensitizers in DSSCs owing to their promising optical and electrochemical properties. The efficiency of DSSCs utilizing these dyes as sensitizers ranged from 4.22 to 6.04%. The *tert*-butyl groups were found to suppress the recombination of injected electrons which contributed to the increment in the photocurrent generation (J_{SC}) and open circuit voltage (V_{OC}). A dye with carbazole donor functionalized with *tert*-butyl groups and the conjugation bridge composed of 2,7-disubstituted carbazole and thiophene fragments exhibited higher V_{OC} value. However, the best device efficiency was observed for a dye with unsubstituted carbazole donor and the π-linker featuring carbazole and bithiophene units due to the high photocurrent generation arising from the facile injection of photogenerated electrons into the conduction band of titanium dioxide (TiO_2) facilitated by the low-lying LUMO.

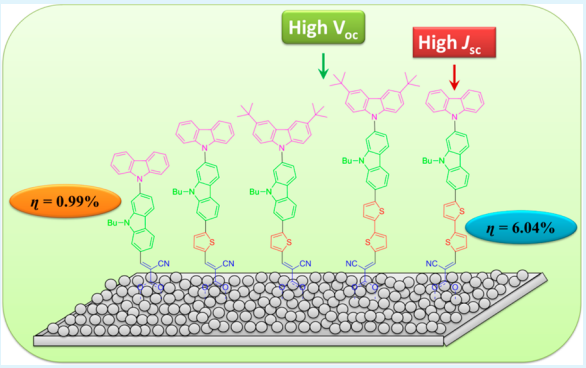

KEYWORDS: *dye-sensitized solar cells, organic dyes, carbazole, absorption, electrochemistry, TDDFT computations*

INTRODUCTION

Organic dyes suitable for application as sensitizers for inorganic semiconductors such as titanium dioxide (TiO_2)[1] and zinc oxide (ZnO)[2] in dye-sensitized solar cells (DSSCs) have received immense attention in recent years due to the possibility that they could serve as low cost consumer power generation equipment in the near future. Performance of DSSCs fabricated using the organic dyes are largely dependent on their electronic and structural characteristics.[3−10] The absorption properties and the frontier orbital energies affect the charge generation and collection efficiency in the devices. Broader and intense charge transfer absorption of the dyes is beneficial for the charge generation, while the LUMO level higher than the conduction band energy of the semiconductor is essential to thermodynamically drive the charge injection.[6] It has been recently found that the recombination of injected electrons with the oxidized dye or the triiodide ions (I_3^-) in electrolyte severely diminishes the photocurrent density.[11] Several structural modifications such as introduction of alkyl chains,[12−15] bridged bianchoring architecture,[16−18] and so forth have been identified to retard the recombination reactions and contribute to the hike in short-circuit current (J_{SC}) and open-circuit voltage (V_{OC}) of the devices. Despite the sincere efforts by chemists in the design of new organic dyes, the DSSCs fabricated using the organic dyes are inferior to those derived from organometallic ruthenium complexes.[10] The reason for the poor performance of organic dyes, despite possessing high molar extinction coefficient for the charge transfer transition, is unclear.[6] In order to unravel this puzzle, more studies on the structure−property relationship on metal free organic dyes are necessary.

Carbazole-based organic materials have been widely employed as active ingredients in electronic devices such as organic light-emitting diodes (OLEDs)[19−21] and DSSCs[22−25] due to their unique charge transporting properties and pronounced thermal stability. Carbazole is an attractive building block as it offers many nuclear sites for functional group incorporation.[26,27] For instance, many carbazole derivatives with functional chromophores attached via C-2, C-3, C-6, C-7, and N-9 have been reported for application in organic light-

Received: November 5, 2013
Accepted: January 23, 2014
Published: January 23, 2014

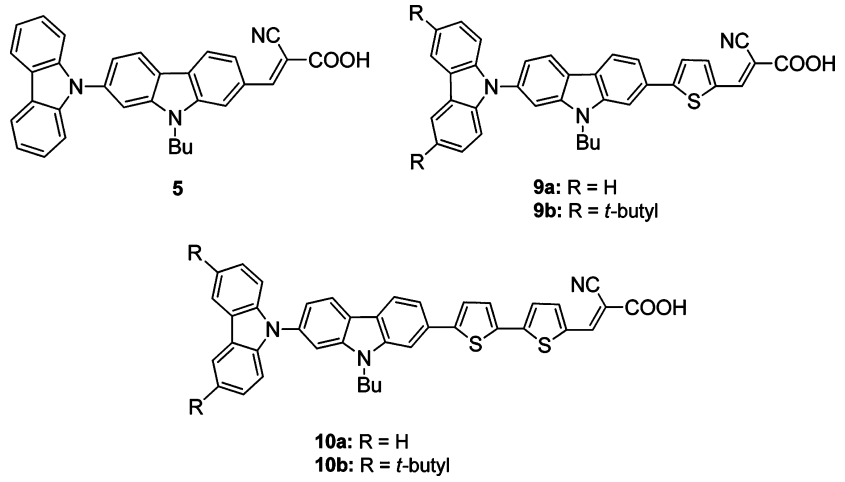

Figure 1. Structures of the new organic dyes containing carbazole as donor and π-linker.

Scheme 1. Synthetic Route to Yield the Dyes

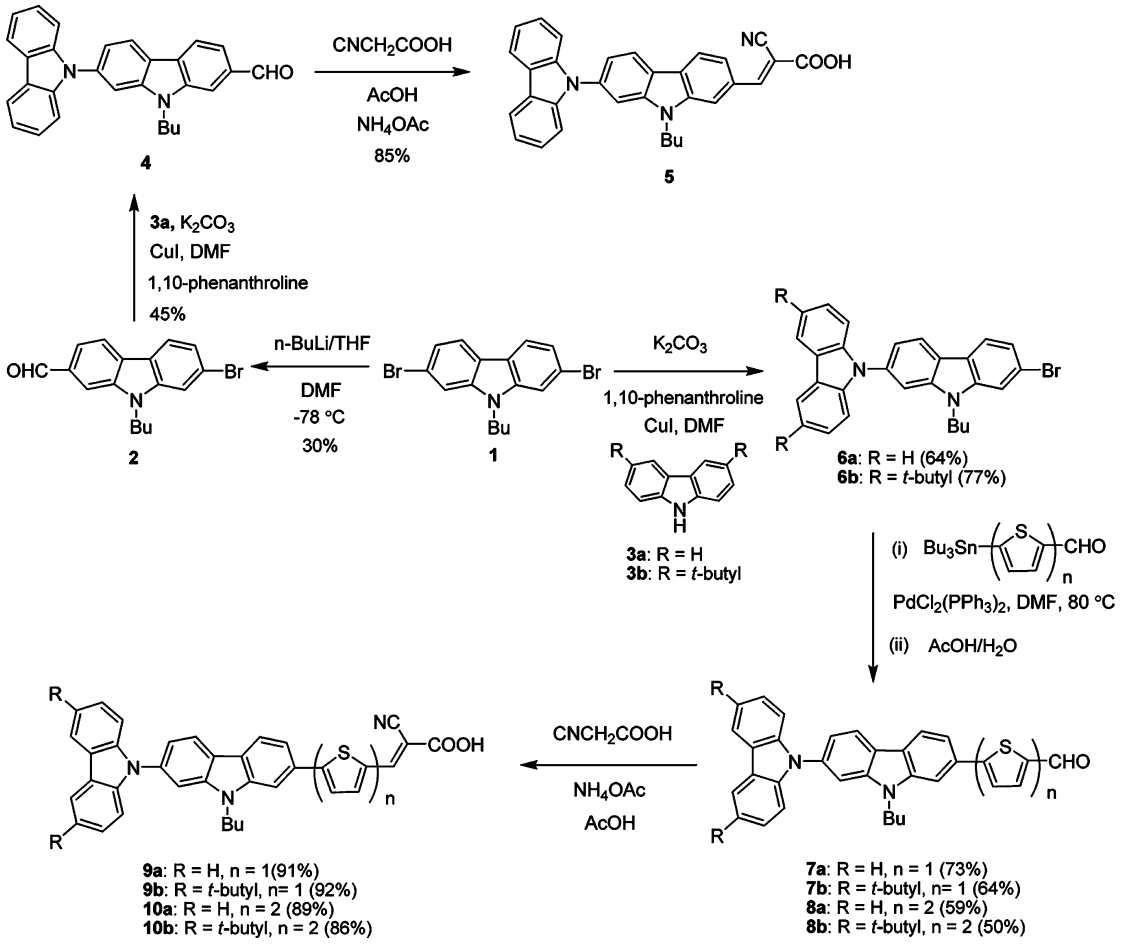

emitting diodes and photovoltaic devices. Particularly, in the dyes serving as sensitizers in DSSCs, carbazole has been used either as a peripheral donor or as a π-linker.[25] Due to the presence of electron rich amine functionality, carbazole can easily donate electron; however, the cation radical formed after the removal of electron is quite unstable owing to the large structural reorganization associated with the oxidation.[28] Substitution of electron releasing groups on the contrary on the carbazole nucleus can enhance the donor strength of the carbazole.[29,30] Keeping all this in mind, we have designed and synthesized a series of metal free organic dyes (Figure 1) containing carbazole as a donor and π-linker. To the best of our knowledge, organic dyes featuring carbazole as donor and 2,7-disubstituted π-linker have not yet been reported.[31] We have studied the effect of substituent variation on the carbazole nucleus as well as the nature of the conjugation bridge on the optical and electrochemical properties. We found that, despite the presence of two carbazole units, additional electron-rich

dx.doi.org/10.1021/am404948w | ACS Appl. Mater. Interfaces 2014, 6, 2528−2539

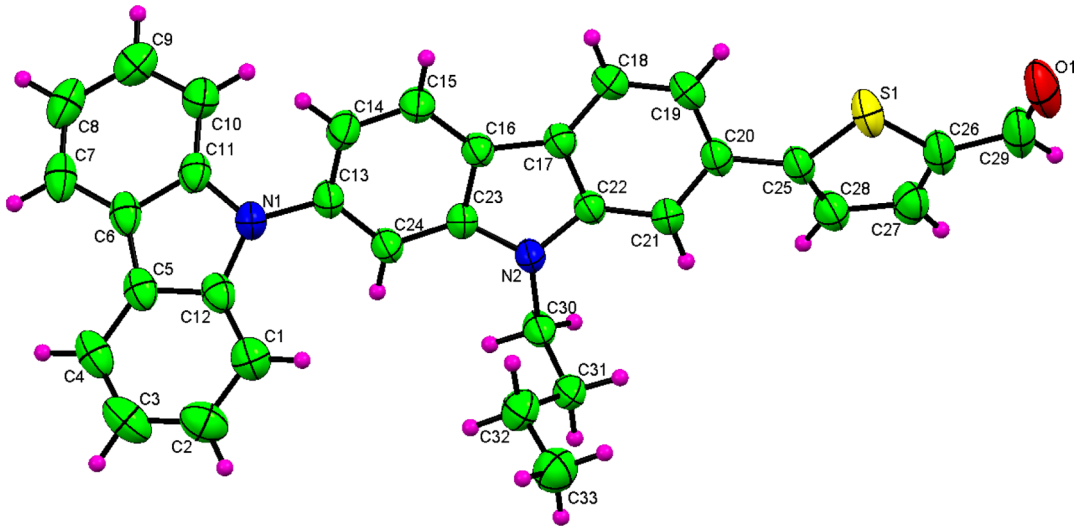

Figure 2. ORTEP plot (50% thermal ellipsoids) of the compound **7a**.

Table 1. Optical and Electrochemical Data of the Dyes and Related Compounds Measured in Dichloromethane

dye	λ_{abs}, nm ($\varepsilon_{max} \times 10^3$ M^{-1} cm^{-1})	λ_{em}, nm	Stokes shift, cm^{-1}[a]	E_{ox}, V[b]	HOMO, eV[c]	LUMO, eV[d]	E_{0-0}, eV[e]	E_{ox}*, V[f]
TC301[h]	374 (12.3)	527	7763	0.90	5.70	2.88	2.82	−1.23
TC302[h]	381 (7.8)	551	8098	0.77	5.57	2.89	2.68	−1.09
BG1[h]	438 (71.0)	585	5737	0.86, 1.35	5.66	3.22	2.44	−0.89
BG2[h]	468 (73.2)	589	4390	0.86, 1.07	5.66	3.33	2.33	−0.78
C1	473 (29.3), 357 (18.0), 311 (16.8), 267 (33.3)	572	3659	0.38 (65), 0.86 (53)	5.18	2.85	2.33	−1.18
C2	489 (34.3), 375 (23.5), 311 (16.9), 264 (34.6)	579	3179	0.33 (52), 0.71 (73)	5.13	2.86	2.27	−1.17
CCT1A	433 (22.0)			0.99	5.79	3.38	2.41	−1.42
CCT2A	457 (23.5)			0.95	5.75	3.53	2.22	−1.27
6a	340 (21.6), 326 (24.0), 294 (21.7)	372, 357	1400	0.80, 1.09	5.60	2.05	3.55	−1.98
6b	342 (25.7), 298 (25.1), 267 (49.3)	381, 374, 367	1992	0.68 (46), 1.14	5.48	1.97	3.51	−2.06
7a	376 (36.6), 294 (24.0)	503	6715	0.79, 1.00	5.59	2.86	2.73	−1.17
7b	383 (35.6), 298 (27.8)	531	7277	0.66 (73), 1.06	5.46	2.67	2.79	−1.36
8a	411 (42.8), 345 (19.7), 294 (19.8)	521	5137	0.70, 0.83	5.50	2.80	2.70	−1.23
8b	411 (41.2), 353 (30.7), 398 (22.3), 266 (47.3)	538	5743	0.64 (99), 0.84	5.44	2.75	2.69	−1.61
5	387 (14.0), 342 (18.2), 293 (22.6), 261 (42.9)	557	7886	0.82, 1.09	5.62	3.16	2.46	−0.87
9a	440 (39.2), 327 (16.0), 293 (20.2), 262 (49.8)	572	5244	0.77	5.57	2.95	2.62	−1.08
9b	443 (40.8), 332 (19.5), 298 (26.7), 259 (61.7)	573	5121	0.66 (68), 1.04	5.46	2.98	2.48	−1.05
10a	476 (45.1), 345 (25.7), 294 (22.2), 262 (61.3)	531	2176	0.67, 0.78	5.47	3.17	2.30	−0.86
10b	478 (44.7), 351 (27.3), 298 (23.8), 258 (59.7)	588	3913	0.62 (73), 0.82	5.42	3.12	2.30	−0.91

[a]From $1/\lambda_{Abs} - 1/\lambda_{em}$. [b]Oxidation potentials are reported with reference to the ferrocene internal standard. [c]Deduced from the oxidation potential using the formula HOMO = 4.8 + E_{ox}. [d]Deduced using the formula LUMO = HOMO − E_{0-0}. [e]Calculated from intersection of absorption and emission spectra. [f]Calculated from E_{ox}* = E_{ox} − E_{0-0}. [h]Recorded in ACN solutions.

thiophene groups were necessary to enhance the functional properties such as optical absorption and redox potentials of this class of dyes. Introduction of electron-rich segments in the conjugation pathway raises the HOMO and LUMO energy and facilitates the regeneration of the dye and electron-injection from the photoexcited dye into the conduction band of TiO_2.[32]

RESULTS AND DISCUSSION

Synthesis and Characterization. The synthetic approach used to prepare the new carbazole-containing dyes is outlined in Scheme 1. The compounds **6a** and **6b** were synthesized by an Ullmann-type coupling[33] of 9*H*-carbazole (**3a**) or 3,6-di-*tert*-butyl-9*H*-carbazole[34] (**3b**) with 2,7-dibromo-9-butyl-9*H*-carbazole[35,36] (**1**) in DMF in the presence of 1,10-phenanthroline, CuI, and K_2CO_3. The corresponding precursor aldehyde derivatives (**7a**−**7b** and **8a**−**8b**) were prepared in moderate yield by Stille coupling reaction[37] between the bromo derivatives (**6a** and **6b**) and the tin reagents of the suitably protected aryl aldehydes and followed by acidic hydrolysis. The dye **5** was prepared by a similar three step reaction pathway. The required aldehyde, 7-bromo-9-butyl-9*H*-carbazole-2-carbaldehyde (**2**), was prepared from **1** by lithiation with *n*-butyl lithium followed by quenching with DMF and subsequent acidic hydrolysis. The aldehyde **4** was also synthesized by Ullmann-type reaction[33] of **2** with 9*H*-carbazole (**3a**). Finally, the aldehydes (**7a**−**7b**, **8a**−**8b**, and **4**) were converted to the corresponding dyes (**9a**−**9b**, **10a**−**10b**, and **5**) in good yields by Knoevenagel condensation reaction[38] with cyanoacetic acid in acetic acid. The dyes are red in color and soluble in dichloromethane, chloroform, toluene, tetrahydrofuran, *N*,*N*-dimethylformamide, and acetonitrile. The dyes were thoroughly characterized by IR, NMR, and mass spectral methods, and the

observed parameters are consistent with the proposed structures.

The structure of the aldehyde **7a** was also confirmed by single crystal X-ray diffraction studies. The ORTEP plot of **7a** is shown in Figure 2. The molecule adopts a noncoplanar geometry in such a way the carbazole and thiophene units are twisted from one another with wide torsion angles. The terminal and bridging carbazole units are tilted from one another with an interplanar angle of 47.49°. The bridging carbazole and thiophene units also deviated from planarity albeit with a smaller interplanar angle of 22.13°. These nonplanar structural arrangement of aromatic π-systems in the conjugation pathway of the dye may be beneficial for the effective charge separation in the excited state[39] and to prevent the aggregation of the dyes at the surface of TiO_2 due to the overall twisted molecular structure.[14] Organic dyes with tilted π-linkers generally displayed enhanced efficiency in the DSSC despite possessing shorter wavelength absorption.[40]

Photophysical Properties. The photophysical behavior of the organic dyes (**5**, **9a**-**9b**, and **10a**−**10b**) was analyzed by recording absorption and fluorescence spectra in five different solvents, for example, dichloromethane (DCM), toluene (Tol), tetrahydrofuran (THF), chloroform ($CHCl_3$), *N*,*N*-dimethylformamide (DMF), and acetonitrile (ACN). The pertinent data are compiled in Table 1 and Table S1 in the Supporting Information, and the absorption spectra recorded for dichloromethane solutions are displayed in Figure 3. In order to understand the origin of absorption in these dyes, the absorption spectra of the precursor compounds, **6**, **7**, and **8** were also measured.

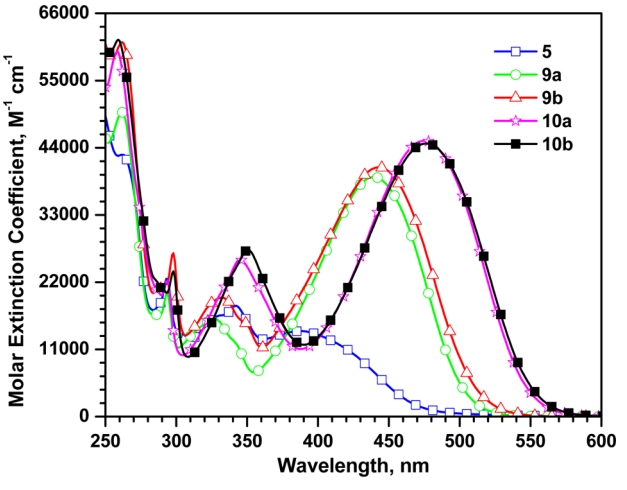

Figure 3. Absorption spectra of the dyes recorded in dichloromethane.

All the dyes show four prominent absorption peaks in the range from 250 to 550 nm (Figure 3). The absorption peaks appearing below 360 nm are either originating from localized $\pi-\pi^*$ transitions or $n-\pi^*$ transitions. The lower energy transition showing absorption maximum above 380 nm corresponds to the charge transfer from the carbazole donor to the cyanoacrylic acid acceptor unit. This band progressively shifted to the longer wavelength region and exhibited enhancement in the molar extinction coefficient on introduction of additional thiophene units in the conjugation pathway. This probably suggests that the charge transfer from carbazole donor to cyanoacrylic acid acceptor is weak due to the poor electron releasing nature of carbazole and incorporation of thiophene units increase the electron-richness of the donor segment due to the delocalization of contributing molecular orbital. Extension of conjugation by oligothiophene units has been found to render a planar bridge between the donor and acceptor and facilitate the donor−acceptor interactions in dipolar compounds.[41,42]

It is interesting to compare the absorption spectral features of these dyes with the closely related dyes possessing phenyl linkages instead of carbazole. Generally, the absorption maxima of the present dyes are red-shifted when compared to the known dyes TC301,[29] TC302,[29] BG-1,[31] BG-2,[31] CCT1A, and CCT2A (Figure 4).[43] Particularly, the longer wavelength absorption realized for the **9b** and **10b** when compared to the analogous dyes CCT1A and CCT2A, respectively, possessing 3,6-disubstituted carbazole as a π-bridge highlights the effective conjugation pathway rendered by the 2,7-disubstituted carbazole. Also the new dyes developed by us showed larger molar extinction coefficient when compared to these dyes. All these observations can be attributed to the electron-richness of the carbazole linker and the facile electronic communication via the 2,7-disubstitution in carbazole.

The nature of the charge transfer transition was confirmed by the following studies. (1) Addition of trifluoroacetic acid (TFA) to dichloromethane solution of the dyes shows a bathochromic shift to the charge transfer absorption. But addition of triethylamine (TEA) leads to a pronounced blue shift for this peak (Figure 5). Such observations have been earlier ascribed to the increment/decrement in acceptor strength on addition of TFA/TEA caused by protonation/deprotonation.[44,45] (2) Also the dyes exhibited longer wavelength absorption when compared to the corresponding bromo- and aldehyde derivatives. The absorption wavelength assumes the order in accordance with the electron-withdrawing effect of the end group (Br < CHO < cyanoacrylic acid). (3) Additionally, all the dyes displayed a negative solvatochromism (Table S1) in the absorption spectra. The blue-shift observed on increasing the polarity of the solvent is attributed to the effective solvation of the dyes.[46,47] However, a drastic blue-shift witnessed for all dyes in DMF is probably due to the basic nature of the solvent which leads to the deprotonation of the dyes.[48] Similarly, the significant red-shift observed in chloro-solvents such as dichloromethane and chloroform arises due to the rapid relaxation of polarizable electrons in the excited state.[49,50]

Though the dyes containing *tert*-butyl groups (**9b** and **10b**) displayed a slight red-shifted absorption in solution, the absorption spectra of the dyes anchored on TiO_2 displayed (Figure 6) a reverse trend. Aggregation at the surface of TiO_2 may produce either blue-shift or red-shift depending on the nature of aggregate formation. Generally, the J aggregates shift the absorption to the longer wavelength region while the H aggregates produce blue-shifted absorption.[51,52] A drastic red-shift in the absorption for the dye **10a** (Figure 6) points to the formation of J aggregates at the surface of TiO_2 probably due to the presence of extended conjugation in the π-linker due to the presence of bithiophene segment. Aggregation behavior of the dye **10a** was also probed by monitoring the changes in the emission spectra on addition of water to the THF solution (Figure S38, Supporting Information). No precipitation was observed by naked eye during the addition of water. The dye exhibited a blue-shift up to 20% of water, and then the spectra progressively shifted to longer wavelength region on increasing the water concentration to 90%. The initial blue-shift may be

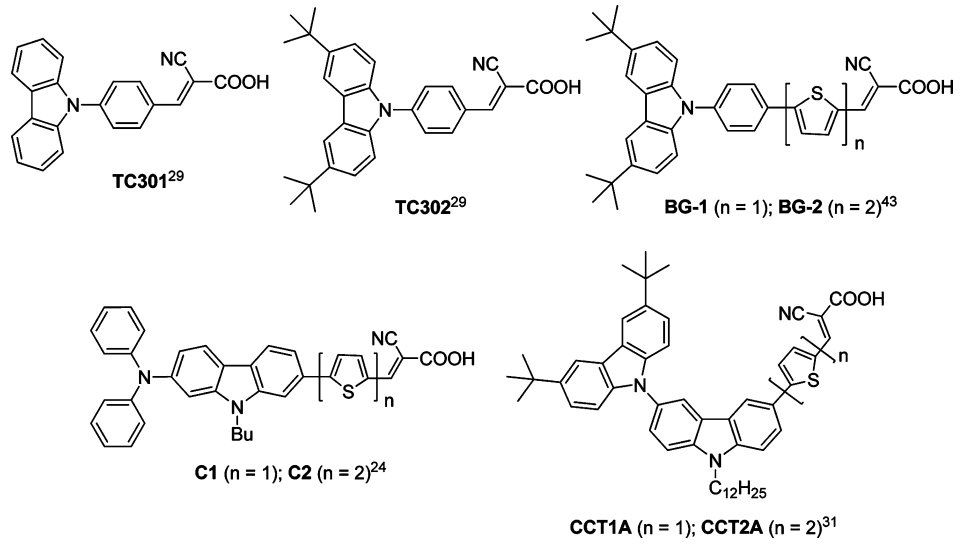

Figure 4. Structures of the related dyes containing carbazole as donor or linker.

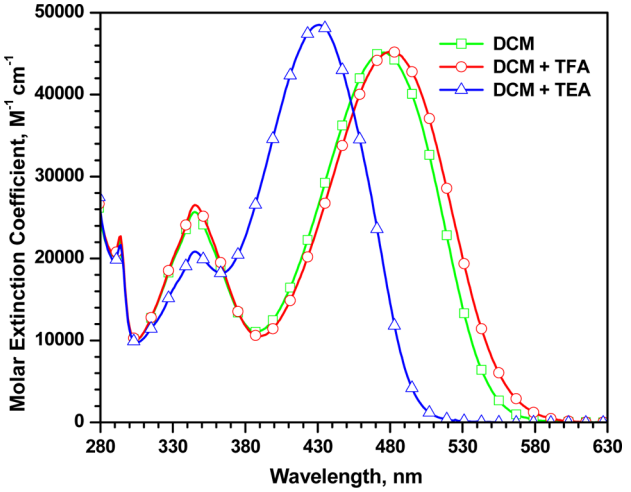

Figure 5. Absorption spectra of the dye **10a** recorded in dichloromethane in the presence of TFA or TEA.

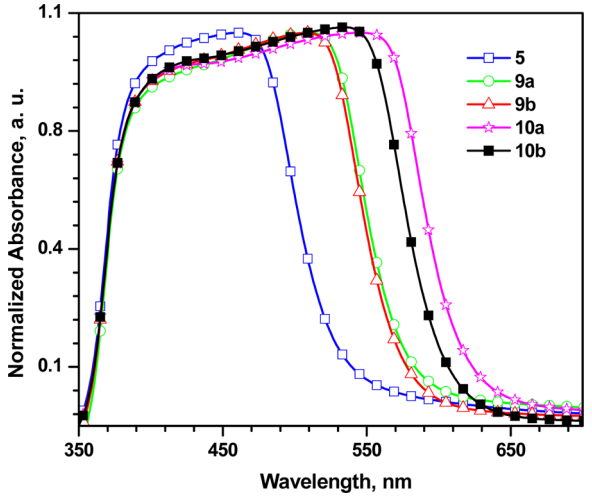

Figure 6. Absorption spectra of the dyes anchored on nanocrystalline TiO_2.

attributed to the hydrogen bonding leading to deprotonation of the carboxylic acid unit.[41] However, the longer wavelength emission observed with 90% water is a clear indication of J aggregate formation. Moreover, the hike in emission intensity at high water concentrations suggests the minimization of nonradiative pathway for the aggregated species which may be beneficial for light harvesting.

Electrochemical Properties. Redox properties of the dyes were estimated by measuring oxidation potentials using cyclic voltammetry in dichloromethane solutions. By comparing the redox potentials of the dyes with oxidation potential of ferrocene measured under same condition we have deduced the energies of the HOMO and LUMO levels of the dyes. From these values, the thermodynamic driving force for electron injection into the conduction band of TiO_2 and regeneration feasibility of the oxidized dyes by electrolyte can be evaluated. The dyes (**9b**, **10b**) possessing *tert*-butyl substituents exhibited reversible oxidation couple (Figure 7) while the remaining dyes showed irreversible oxidation peaks. The redox potentials of the later dyes were estimated from differential pulse voltammetric studies. The reversibility

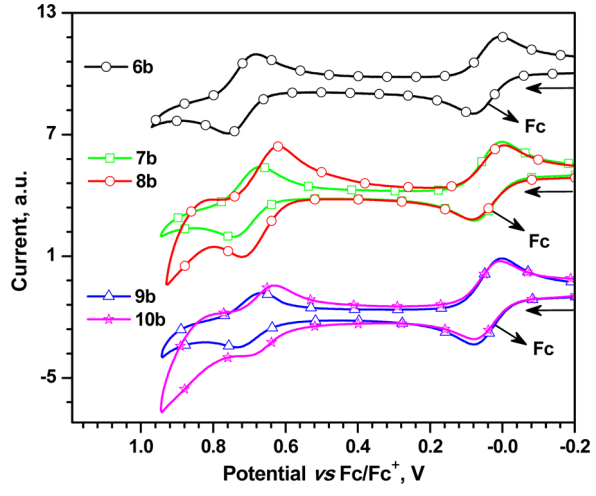

Figure 7. Cyclic voltammograms of the dyes recorded in dichloromethane solutions.

dx.doi.org/10.1021/am404948w | ACS Appl. Mater. Interfaces 2014, 6, 2528−2539

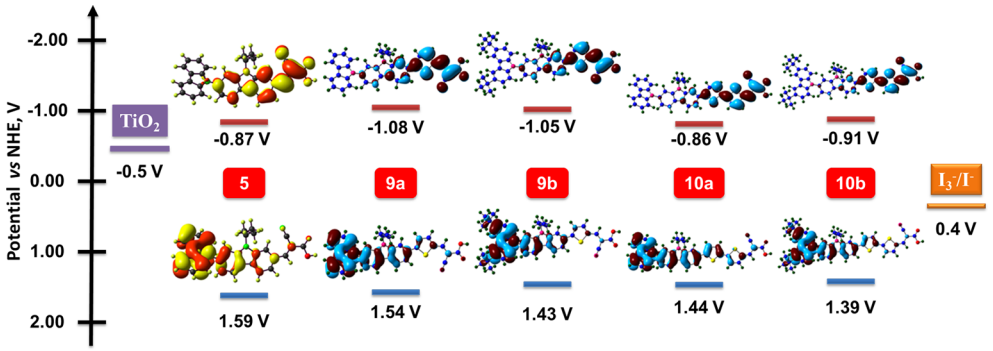

Figure 8. Energy level diagram showing the ground and excited state oxidation potentials observed for the dyes.

Table 2. Performance Parameters of the DSSCs Fabricated Using the Dyes

dye	J_{SC}, mA cm^{-2}	V_{OC}, mV	*ff*	η (%)	R_{rec}, Ω	R_{ct2}, Ω	f_{max}, Hz	τ_e, ms
5	2.79 ± 0.17	555 ± 10.07	0.64 ± 0.01	0.99 ± 0.05	26.62	70.35	93.3	1.7
9a	9.98 ± 0.19	635 ± 4.62	0.66 ± 0.01	4.22 ± 0.06	43.73	26.12	46.5	3.4
9b	11.22 ± 0.11	666 ± 3.46	0.66 ± 0.00	4.95 ± 0.04	47.11	25.55	26.5	6.2
10a	15.78 ± 0.25	601 ± 3.06	0.64 ± 0.01	6.04 ± 0.02	36.59	20.93	107.2	1.5
10b	14.00 ± 0.27	612 ± 2.65	0.64 ± 0.01	5.48 ± 0.01	42.10	23.03	70.5	2.3
N719	17.60	724	0.66	8.44				

observed for the dyes **9b** and **10b** may be ascribed to the hindrance for dimerization of cation radicals formed on oxidation. Unsubstituted carbazoles undergo facile dimerization at C-3 and C-6 positions.[53] The presence of *tert*-butyl groups at C-3,C-6 positions in the present dyes suppresses the dimerization of the radical cations formed on oxidation.[54] Also the facile oxidation of **9b** and **10b** when compared to the rest may be attributed to the electron-releasing propensity of *tert*-butyl groups.[29] It is interesting that the HOMO and LUMO energies of these dyes can be fine-tuned by changing the substituents on the donor carbazole and nature of the linker (Figure 8). The ground state oxidation potentials of the dyes are in the range of 1.39−1.59 V vs NHE. The oxidation potentials of the dyes were raised on elongation of the conjugation by thiophene and bithiophene insertion and donor strength by introduction of *tert*-butyl groups on carbazole. Moreover, the dyes possess oxidation potential more positive than redox potential of the iodine/iodide electrolyte (0.4 V vs NHE) commonly employed in DSSC fabrication. This suggests that the dyes can be easily regenerated by the electrolyte. The first excited state oxidation potential of the dyes is located in the range −0.86 to −1.08 V. These values are more negative than the conduction band edge of TiO_2 (−0.5 V vs NHE).[55] There exists at least 0.36 V difference which is sufficient to provide the required thermodynamic driving force for the injection of the photogenerated electrons from the dye into the conduction band of TiO_2.[10] Since the dyes possess desirous ground and excited state potentials, they are expected to serve as efficient sensitizers in nanocrystalline TiO_2-based dye-sensitized solar cells. Particularly the dyes **9a** and **9b** are expected to show enhanced electron injection rate. However, the longer wavelength intense absorption observed for the dyes **10a** and **10b** may be beneficial to generate more photocurrent.

Theoretical Calculations. To gain further insight into the electronic structure of the dyes, we have optimized the geometry of the dyes by density functional theory (DFT)[56] at the level B3LYP/6-31 G (d, p)[56] and computed the vertical excitation energies using MPW1K/6-31 G (d, p)[57] because this theoretical treatment gave reliable estimate on the absorption parameters for the donor−acceptor compounds, particularly the organic sensitizers possessing D-π-A molecular configuration. The computed parameters are listed in Table S2 in the Supporting Information and the electronic distribution observed for the frontier molecular orbitals are also shown in Figure 8. The HOMOs of the dyes are mainly contributed by the carbazole fragments (donor and linker) and it is spread up to one of the thiophenes in the dyes containing bithiophene unit in the conjugation pathway (Figure 8). However, the LUMO is precisely located on the thiophene cyanoacrylic acid segment for the dyes possessing thiophene units in the conjugation pathway. The carbazole linker also contributed to the LUMO of the dye **5**. The HOMO and LUMO of the dyes were well separated in the dyes **9** and **10** which favor a facile charge migration from the donor to acceptor on irradiation at the CT transition. However, for the dye **5**, the HOMO and LUMO are overlapping significantly and suggest a poor charge transfer propensity. Due to this, the dye **5** exhibited poor performance in the DSSC (*vide supra*).

DSSC Characteristics. Since the organic dyes showed interesting absorption and electrochemical properties suitable to perform as sensitizers in TiO_2-based dye-sensitized solar cells, we have tested their response in the DSSC by using photoanodes derived from the dyes. Photovoltaic performances of the DSSCs are tabulated in Table 2. The *I*−*V* characteristics observed for the devices under simulated solar light irradiation are displayed in Figure 9. The DSSC based on dye **10a** exhibited high photocurrent while that of the dye **9b** displayed high V_{OC} in the series. However, the dye **5** showed low J_{SC} and V_{OC} in DSSC. The poor performance of **5** in DSSC is attributed to the weak charge transfer transition appearing below 400 nm which probably reduces the electron generation propensity of the dye. Also, it possesses relatively small thermodynamic driving force for electron injection into the conduction band of TiO_2. Consequently, less electron generation and less favorable electron injection reduce the electron density in the conduction band of TiO_2. In general, V_{OC} of the thiophene derivatives **9a** and **9b** are larger than the analogous bithiophene counterparts **10a** and **10b**. This is again

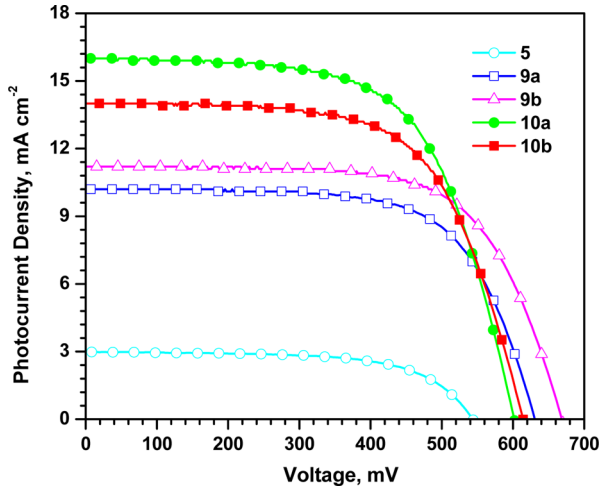

Figure 9. *I*–*V* characteristics of the DSSCs fabricated using the dyes.

rationalized as originating from the favorable electron injection possible for these dyes due the more positive LUMO. There is also some interesting outcome due to the structural modification on carbazole donor. The dyes **9b** and **10b** containing *tert*-butyl substituents displayed larger V_{OC} when compared to the corresponding unsubstituted dyes **9a** and **10a**. This probably is due to the slightly enhanced light-harvesting property of the former dyes when compared to the later and the *tert*-butyl groups retarding the recombination of TiO_2 conduction band electrons with the triiodide ions (I_3^-) in electrolyte by rendering hydrophobic environment which prevent the approach of the triiodide ions to TiO_2.

Incident photon-to-current conversion efficiency (IPCE) measured against the wavelength of irradiation for the DSSCs are displayed in Figure 10. All the dyes exhibited exceptional

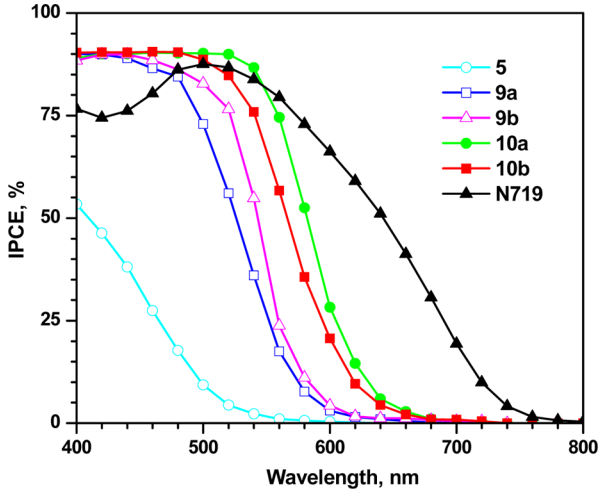

Figure 10. IPCE plots of the DSSCs fabricated using the dyes.

photon-to-electron conversion efficiency in the wavelength region from 400 to 600 nm. The action spectra are largely in accordance with the absorption band profile observed for the dyes in the solid state (Figure 6). The present dyes showed very high IPCE in the 400–500 nm region which is complementary to the ruthenium-based organometallic dyes such as N719[58] and ascribed to the high molar extinction coefficients observed for the dyes in that region. The power conversion efficiencies of all the compounds are higher than 4% except the dye **5**. The device based on the dye **10a** exhibited a short circuit current density (J_{SC}) of 15.78 ± 0.25 mA cm^{-2}, open circuit voltage (V_{OC}) of 601 ± 3.06 V, fill factor (*ff*) of 0.64 ± 0.01, and power conversion efficiency of 6.04 ± 0.02%. The J_{SC} of the dyes follows the order **5** < **9a** < **9b** < **10b** < **10a** consistent with the absorption spectra observed for the dyes anchored on TiO_2 (*vide supra*). The larger photocurrent observed for the DSSC based on the dye **10a** may be attributed to the longer wavelength light harvesting ability arising from the aggregated species (*vide supra*) and the retardation of electron recombination with the electrolyte. However, for the dye **10b**, though the conjugation segment is very similar to that in **10a**, the aggregation and electron recombination are retarded by the bulky *tert*-butyl groups. Similarly, the V_{OC} for the devices show the order: **5** < **10a** < **10b** < **9a** < **9b**. It is interesting that the dyes possessing bithiophene in the conjugation (**10**) displayed low V_{OC} than the corresponding dyes with short conjugation (**9**). It is well documented in the literature that organic dyes possessing extended conjugation normally show enhanced photocurrent at the expense of photovoltage attributable to the reduction in the electron density in the conduction band of TiO_2.[43]

To understand the fate of the photogenerated electrons, detailed electrochemical impedance spectroscopy was performed on the DSSCs fabricated using the dyes. Nyquist plots of the DSSCs measured under dark and illumination conditions are displayed in Figure 11. Figure 11a, which corresponds to dark conditions, displays three semicircles for all DSSCs and each semicircle corresponds to the resistance experienced at a particular interface of the components present in the DSSC device. The larger semicircle corresponds to the recombination resistance at TiO_2/dye/interface and the radius of this semicircle follows the order **10b** < **10a** < **9b** < **9a** < **5**. Smaller R_{rec} value is indicative of faster electron recombination and may result in a comparatively small open-circuit voltage.[59,60] The R_{rec} for the devices follow the order, **5** < **10a** < **10b** < **9a** < **9b**. On this basis, **5** is expected to display small V_{OC} while **9b** may produce high V_{OC}. The oxidation potential of the dye and the charge-recombination resistance can alter the electron density in TiO_2.[61] Dyes that undergo oxidation more easily may increase the polarizability of the molecule and enhance the electron density on TiO_2. Relatively low oxidation potentials observed for the dyes **9b**, **10a**, and **10b** suggest favorable interfacial interaction between TiO_2 and dye. In accordance with this hypothesis, the electron transport resistance (R_{ct2}) estimated from the Nyquist plots recorded under illumination conditions (Figure 11b) was relatively low for them (**5** > **9a** > **9b** > **10b** > **10a**). The electron lifetime ($\tau_e = 1/\omega_{min} = 1/2\pi f_{max}$, where f_{max} is the maximum frequency of the low-frequency peak) in the Bode phase plot is highest for **9b** (**10a** < **5** < **10b** < **9a** < **9b**). The highest τ_e observed for **9b** is suggestive of effective suppression of back reaction of injected electrons with I_3^- ions in the electrolyte. Thus, the comparatively high V_{OC} observed for the thiophene conjugated dyes **9a** and **9b** may be attributed to the electron collection efficiency in their DSSCs due to the retardation of recombination of electron.

CONCLUSION

We have successfully synthesized five new organic dyes featuring carbazole/3,6-di(*tert*-butyl) carbazole donor, 2,7-carbazole linker, and cyanoacrylic acid acceptor. Dyes containing thiophene or bithiophene in the conjugation

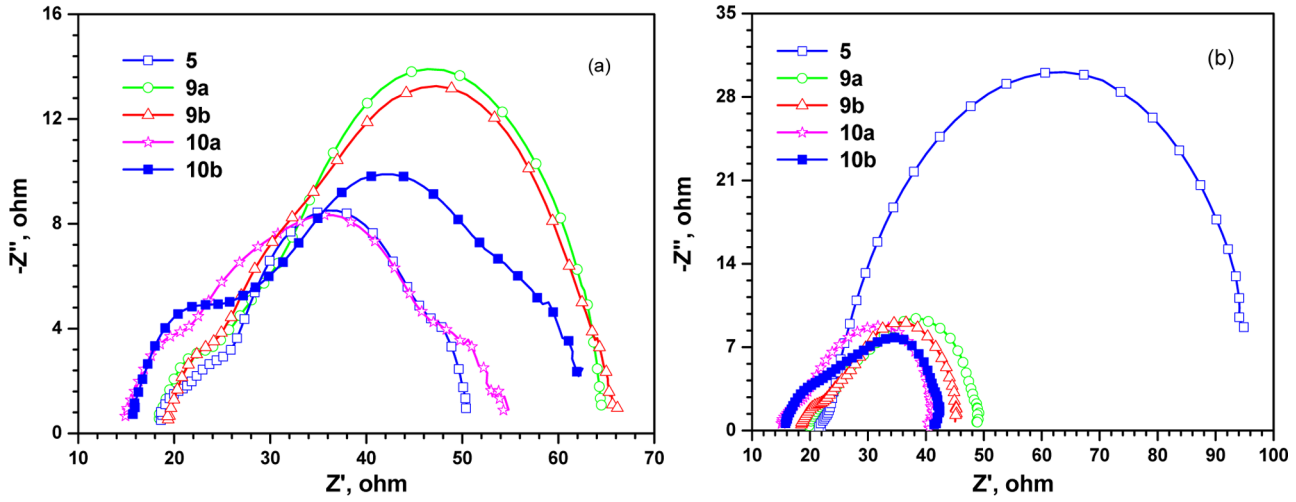

Figure 11. Nyquist plots observed for the DSSCs measured under (a) dark and (b) illumination conditions.

pathway in addition to carbazole were also synthesized. All these dyes displayed high molar extinction coefficients for the charge-transfer transition and suitable LUMO and HOMO energy levels which facilitate the transfer of electron from the excited state of the dye into the conduction band of TiO_2 and the regeneration of the oxidized dyes by electrolyte. The dyes showed improved light-harvesting properties when compared to the analogous dyes possessing 3,6-carbazole (**CCT1A** and **CCT2A**) or phenyl (**BG-1** and **BG-2**) linker. This establishes the supremacy of the 2,7-carbazole as an effective π-conjugation pathway when compared to the similar chromophores. The DSSC based on a dye **10a** exhibited J_{SC} = 15.78 ± 0.25 mA cm^{-2}, V_{OC} = 601 ± 3.06 V, *ff* = 0.64 ± 0.01, and overall power conversion efficiency of 6.04 ± 0.02% owing to the balance in the absorption properties and electron collection efficiency.

EXPERIMENTAL SECTION

General Methods. All the precursor compounds required for the work were purchased from commercial sources and used without further purification. However, the solvents were purified and dried by standard procedures prior to use. Column chromatography purifications were performed with silica gel (230−400 mesh) as a stationary phase in a column with 40 cm long and 3.0 cm diameter. The IR spectra were recorded with a spectrophotometer using KBr pellets. The ^{1}H and ^{13}C NMR spectra were recorded with a NMR spectrometer operating at 500.13 and 125.77 MHz respectively. Deuterated chloroform ($CDCl_3$) and dimethyl sulfoxide (DMSO-d_6) were used as solvent for the measurements and the calibration performed using the residual peak of the deuterated solvents (δ 7.26 and 2.52 for ^{1}H; 77.0 and 39.5 for ^{13}C). UV−vis spectra were recorded at room temperature in quartz cuvettes using a UV−vis spectrophotometer in the range 250−1100 nm. Emission spectra were recorded using a spectrofluorimeter at room temperature for the air equilibrated solutions. Cyclic voltammetry (CV) and differential pulse voltammetry (DPV) were performed on an electrochemical workstation using a three electrode assembly comprising glassy carbon working electrode, a nonaqueous $Ag/AgNO_3$ reference electrode and an auxiliary platinum electrode. The experiments were performed at room temperature under nitrogen atmosphere in dichloromethane using 0.1 M tetrabutylammonium perchlorate (Bu_4NClO_4) as supporting electrolyte. The high resolution mass spectra of the compounds were obtained from a HRMS ESI mass spectrometer in the positive ion mode.

7-Bromo-9-butyl-9*H*-carbazole-2-carbaldehyde (2). A solution of 2,7-dibromo-9-butyl-9*H*-carbazole (**1**, 3.78 g, 10 mmol) in dry tetrahydrofuran (60 mL) was cooled to −78 °C and a solution of *n*-butyl lithium in hexane (7.0 mL, 1.6 M) was added dropwise over 15 min. After the addition was over, it was stirred for additional 1 h and treated with DMF (1.5 mL). The reaction mixture was slowly allowed to attain room temperature and continued to stir overnight. Finally, the volatiles were removed by vacuum evaporation and the residue triturated with aqueous ammonium chloride solution. The organic soluble content was extracted with dichloromethane, dried over anhydrous sodium sulfate and evaporated to yield the crude product. It was purified by column chromatography on silica gel by using hexane/dichloromethne (2:3) as an eluent. White solid. Yield: 0.99 g (30%); mp 90−92 °C. IR (KBr, cm^{-1}) 1692 ($\nu_{C=O}$). ^{1}H NMR ($CDCl_3$, 500.13 MHz) δ 10.16 (s, 1H), 8.17 (d, *J* = 8.0 Hz, 1H), 7.95−8.00 (m, 2H), 7.75−7.76 (d, *J* = 8.0 Hz, 1H), 7.60 (s, 1H), 7.38 (dd, *J* = 8.5 Hz, 1.5 Hz, 1H), 4.32 (t, *J* = 7.5 Hz, 2H), 1.86 (quin, *J* = 7.5 Hz, 2H), 1.4 2 (quin, *J* = 3.0 Hz, 2H), 0.97 (t, *J* = 7.5 Hz, 3H). ^{13}C NMR ($CDCl_3$, 125.77 MHz) δ 192.6, 142.9, 140.3, 134.1, 127.5, 122.9, 122.6, 121.8, 121.5, 120.8, 120.6, 112.3, 109.8, 43.3, 31.1, 20.6, 13.9. HRMS calcd for $C_{17}H_{17}BrNO$ $[M+1]^+$ *m*/*z* 330.0488, found 330.0487.

9-Butyl-7-(9*H*-carbazol-9-yl)-9*H*-carbazole-2-carbaldehyde (4). A mixture of 9*H*-carbazole (**3a**, 0.19 g, 1.12 mmol), CuI (0.03 g, 15 mol %), 1,10-phenanthroline dihydrate (0.04 g, 20 mol %), anhydrous K_2CO_3 (0.41 g, 3 mmol), 7-bromo-9-butyl-9*H*-carbazole-2-carbaldehyde (**2**, 0.38 g, 1 mmol), and DMF (10 mL) was refluxed for 24 h under nitrogen atmosphere. On completion of the reaction, the reaction mixture was extracted with dichloromethane, washed with brine solution and dried over anhydrous sodium sulfate. On evaporation of the dichloromethane solution a tan yellow residue was obtained. It was purified by column chromatography on silica gel using hexane/dichloromethane (2:3) as an eluent. Light yellow solid. Yield: 0.19 g (45%); mp 122−124 °C. IR (KBr, cm^{-1}) 1693 ($\nu_{C=O}$). ^{1}H NMR ($CDCl_3$, 500.13 MHz) δ 10.20 (s, 1H), 8.34 (d, *J* = 8.5 Hz, 1H), 8.28 (d, *J* = 8.0 Hz, 1H), 8.18 (d, *J* = 3.0 Hz, 2H), 8.02 (s, 1H), 7.82 (d, *J* = 8.0 Hz, 1H), 7.64 (s, 1H),7.48 (t, *J* = 7.5 Hz, 3H), 7.44 (t, *J* = 8.5 Hz, 2H), 7.32 (t, *J* = 7.0 Hz, 2H), 4.38 (t, *J* = 7.5 Hz, 2H), 1.86−1.90 (m, 2H), 1.40−1.44 (m, 2H), 0.93−0.97 (m, 2H). ^{13}C NMR ($CDCl_3$, 125.77 MHz) δ 192.5, 143.0, 141.2, 140.9, 137.2, 134.1, 127.8, 123.5, 122.9, 122.7, 122.6, 121.9, 121.1, 120.7, 120.6, 118.9, 109.8, 109.8, 107.9, 43.3, 31.1, 20.6, 13.9. HRMS calcd for $C_{29}H_{24}N_2ONa$ $[M+Na]^+$ *m*/*z* 439.1780, found 439.1797.

(*E*)-3-(9-Butyl-7-(9*H*-carbazol-9-yl)-9*H*-carbazol-2-yl)-2-cyanoacrylic Acid (5). The aldehyde **4** (0.14 g, 0.33 mmol), 2-cyanoacetic acid (0.04 g, 0.5 mmol), ammonium acetate (0.04 g, 0.25 mmol), and acetic acid (5 mL) were mixed and refluxed for 24 h. The resulting red precipitate was filtered and washed several times with water and dried. It was crystallized from dichloromethane/hexane mixture to obtain the analytically pure sample. Yellow solid. Yield: 0.14 g (85%); mp 155 °C. IR (KBr, cm^{-1}) 1600 ($\nu_{C\equiv N}$). ^{1}H NMR ($CDCl_3$, 500.13 MHz) δ 8.50 (s, 1H), 8.24 (m, 1H), 8.14−8.20 (m, 3H), 7.58

(d, J = 9.5 Hz, 1H), 7.37−7.49 (m, 5H), 7.30−7.34 (m, 2H), 4.31−4.33 (m, 2H), 1.85−1.88 (m, 2H), 1.39−1.44 (m, 2H), 0.92−0.97 (m, 3H). ^{13}C NMR ($CDCl_3$, 125.77 MHz) δ 142.9, 141.3, 141.2, 140.9, 137.2, 125.9, 125.89, 125.86, 123.4, 123.3, 122.4, 120.7, 120.32, 120.27, 120.0, 119.82, 119.79, 118.71, 109.68, 107.58, 43.1, 31.5, 20.5, 13.8. HRMS calcd for $C_{32}H_{25}N_3O_2$ $[M]^+$ m/z 483.1941, found 483.1972.

2-Bromo-9-butyl-7-(9*H*-carbazol-9-yl)-9*H*-carbazole (6a). It was prepared from **1** (7.56 g, 20 mmol) and **3b** (1.67 g, 10 mmol) by following a procedure described above for **4**. White solid. Yield: 3.18 g (64%); mp 182−184 °C. ^{1}H NMR ($CDCl_3$, 500.13 MHz) δ 8.23 (d, J = 8.0 Hz, 1H), 8.18 (d, J = 7.5 Hz, 1H), 8.0 (d, J = 8.0 Hz, 1H), 7.59 (d, J = 1.5 Hz, 1H), 7.56 (d, J = 1.5 Hz, 1H), 7.46 (d, J = 8.0 Hz, 2H), 7.39−7.48 (m, 4H), 7.31−7.33 (m, 2H), 4.25 (t, J = 7.0 Hz, 2H), 1.82−1.85 (m, 2H), 1.37−1.42 (m, 2H), 0.92−0.95 (m, 3H). ^{13}C NMR ($CDCl_3$, 125.77 MHz) δ 141.3, 126.0, 123.4, 122.6, 121.6, 121.5, 120.4, 119.9, 118.7, 112.1, 109.9, 107.8, 43.3, 31.1, 20.6, 13.9. HRMS calcd for $C_{28}H_{24}BrN_2$ $[M+1]^+$ m/z 467.1117, found 467.1110.

9-(7-Bromo-9-butyl-9*H*-carbazol-2-yl)-3,6-di-*tert*-butyl-9*H*-carbazole (6b). It was prepared from 3,6-di-*tert*-butyl-9*H*-carbazole (**3b**, 1.68 g, 6 mmol) and **1** (4.54 g, 12 mmol) by following a procedure described above for **6a**. White solid; Yield: 2.68 g (77%); mp 102−104 °C. ^{1}H NMR ($CDCl_3$, 500.13 MHz) δ 8.19−8.22 (m, 3H), 7.99−8.00 (d, J = 8.0 Hz, 1H), 7.58 (d, J = 15.0 Hz, 2H), 7.48−7.50 (d, J = 8.5 Hz, 2H), 7.39−7.43 (m, 4H), 4.26 (t, J = 6.5 Hz, 2H), 1.84 (t, J = 7.0 Hz, 2H), 1.49 (s, 18H), 1.39−1.41 (m, 2H), 0.95 (t, J = 7.0 Hz, 3H). ^{13}C NMR ($CDCl_3$, 125.77 MHz) δ 142.8, 141.9, 141.4, 139.7, 136.6, 123.6, 123.3, 122.5, 121.58, 121.55, 121.4, 121.3, 119.5, 118.5, 116.3, 112.0, 109.3, 107.4, 43.3, 34.8, 32.1, 31.1, 20.6, 13.9. HRMS calcd for $C_{36}H_{39}BrN_2$ $[M]^+$ m/z 578.2291, found 578.2292.

5-(9-Butyl-7-(9*H*-carbazol-9-yl)-9*H*-carbazol-2-yl)thiophene-2-carbaldehyde (7a). A mixture of (5-(1,3-dioxolan-2-yl)thiophen-2-yl)tributylstannane (0.49 g, 1.1 mmol), **6a** (0.47 g, 1 mmol), and dry DMF (5 mL) was maintained under nitrogen atmosphere and $Pd(PPh_3)_2Cl_2$ (0.01 g, 0.01 mmol) added to it. The resulting reaction mixture was heated at 80 °C for 15 h. After the completion of reaction, the reaction mixture was poured into cold water and extracted with dichloromethane (3 × 40 mL). Removal of volatiles from the dichloromethane extract by rotary evaporation produced a solid residue. It was dissolved in glacial acetic acid (4 mL) and heated at 60 °C for 1 h to form a clear solution. After the addition of water (3 mL) the reaction mixture was maintained at 60 °C for additional 1 h. Finally, it was extracted with dichloromethane (3 × 40 mL). The dichloromethane extract was washed thoroughly with brine solution and dried over anhydrous sodium sulfate. The solid residue obtained on evaporation of the dichloromethane extract was purified by column chromatography on silica gel by using hexane/dichloromethane mixture (1:1) as an eluant. Yellow solid. Yield: 0.36 g (73%); mp 120−122 °C. IR (KBr, cm^{-1}) 1656 ($\nu_{C=O}$). ^{1}H NMR ($CDCl_3$, 500.13 MHz) δ 9.93 (s, 1H) 8.28 (d, J = 8.0 Hz, 1H), 8.18−8.20 (m, 2H), 7.80 (d, J = 4.0 Hz, 1H), 7.73 (d, J = 1.0 Hz, 1H), 7.63 (dd, J = 8.5 Hz, 1.5 Hz, 1H), 7.60 (d, J = 1.5 Hz, 1H), 7.55 (d, J = 4.0 Hz, 1H), 7.50 (d, J = 8.0 Hz, 2H), 7.42−7.46 (m, 2H), 7.31−7.34 (m, 2H), 4.36 (t, J = 7.0 Hz, 2H), 1.87−1.92 (m, 2H), 1.40−1.47 (m, 2H), 0.96 (t, J = 7.5 Hz, 3H). ^{13}C NMR ($CDCl_3$, 125.77 MHz) δ 182.7, 155.6, 142.3, 142.1, 141.5, 141.3, 137.5, 136.1, 130.9, 126.0, 124.2, 123.7, 123.4, 121.8, 121.7, 121.1, 120.4, 120.0, 118.7, 118.2, 109.9, 107.8, 106.8, 43.2, 31.2, 20.6, 13.9. HRMS calcd for $C_{33}H_{26}N_2OSNa$ $[M+Na]^+$ m/z 521.1658, found 521.1658.

5-(5-(9-Butyl-7-(9*H*-carbazol-9-yl)-9*H*-carbazol-2-yl)-thiophen-2-yl)thiophene-2-carbaldehyde (8a). Compound **8a** was synthesized in 59% yield (0.34 g) from **6a** (0.47 g, 1 mmol) and (5-(5-(1,3-dioxolan-2-yl)thiophen-2-yl)thiophen-2-yl)tributylstannane (0.58 g, 1.1 mmol) by following a procedure similar to that described above for **7a**. Yellow solid; mp 158−160 °C. IR (KBr, cm^{-1}) 1651 ($\nu_{C=O}$). ^{1}H NMR ($CDCl_3$, 500.13 MHz) δ 9.88 (s, 1H), 8.26−8.27 (d, J = 8.0 Hz, 1H), 8.18−8.20 (d, J = 7.5 Hz, 2H), 8.15−8.17 (d, J = 8.5 Hz, 1H), 7.70 (d, J = 4.0 Hz, 1H), 7.647 (s, 1H), 7.56−7.58 (m, 2H), 7.46 (d, J = 8.0 Hz, 2H), 7.40−7.45 (m, 5H), 7.30−7.33 (m, 3H), 4.35 (t, J = 7.0 Hz, 2H), 1.89 (quin, J = 7.5 Hz, 2H), 1.41−1.46 (m, 2H), 0.96 (t, J = 7.0 Hz, 3H). ^{13}C NMR ($CDCl_3$, 125.77 MHz) δ 181.5, 146.4, 146.3, 141.0, 140.6, 140.6, 140.4, 136.6, 134.8, 134.0, 130.4, 126.3, 125.1, 123.4, 123.0, 122.4, 121.8, 120.9, 120.6, 120.1, 119.5, 119.0, 117.6, 116.9, 109.0, 106.7, 105.1, 42.2, 30.3, 19.7, 13.0. HRMS calcd for $C_{37}H_{28}N_2OS_2$ $[M]^+$ m/z 580.1637, found 580.1637.

5-(9-Butyl-7-(3,6-di-*tert*-butyl-9*H*-carbazol-9-yl)-9*H*-carbazol-2-yl)thiophene-2-carbaldehyde (7b). It was synthesized from **6b** (0.58 g, 1 mmol) and (5-(1,3-dioxolan-2-yl)thiophen-2-yl)-tributylstannane (0.49 g, 1.1 mmol) in 64% yield (0.39 g) by following a procedure similar to that described above for **7a**. Yellow solid; mp 137−138 °C. IR (KBr, cm^{-1}) 1660 ($\nu_{C=O}$). ^{1}H NMR ($CDCl_3$, 500.13 MHz) δ 9.93 (s, 1H), 8.25 (s, 1H), 8.17−8.19 (m, 3H), 7.81 (d, J = 3.5 Hz, 1H), 7.72 (s, 1H), 7.62 (dd, J = 8.0 Hz, 1.5 Hz, 1H), 7.59 (d, J = 1.5 Hz, 1H), 7.55 (d, J = 4.0 Hz, 1H), 7.49 (dd, J = 8.5 Hz, 2H), 7.43−7.45 (m, 3H), 4.35 (t, J = 7.5 Hz, 3H), 1.85−1.91 (m, 2H), 1.49 (s, 18 H), 1.41−1.44 (m, 2H), 0.94−0.97 (m, 3H). ^{13}C NMR ($CDCl_3$, 125.77 MHz) δ 182.8, 155.6, 142.9, 142.2, 142.1, 141.4, 139.6, 137.6, 136.6, 130.7, 124.1, 123.7, 123.7, 123.4, 121.7, 121.3, 121.1, 118.5, 118.1, 116.4, 109.3, 107.3, 106.7, 43.2, 34.8, 32.1, 31.2, 20.6, 14.0. HRMS calcd for $C_{41}H_{42}N_2OS$ $[M]^+$ m/z 610.3012, found 610.3004.

5-(5-(9-Butyl-7-(3,6-di-*tert*-butyl-9*H*-carbazol-9-yl)-9*H*-carbazol-2-yl)thiophen-2-yl)thiophene-2-carbaldehyde (8b). It was obtained from **6b** (0.58 g, 1 mmol) and (5-(5-(1,3-dioxolan-2-yl)thiophen-2-yl)thiophen-2-yl)tributylstannane (0.58 g, 1.1 mmol) by following a procedure similar to that described above for **7a**. Yellow solid. Yield: 50% (0.35 g); mp 166−168 °C. IR (KBr, cm^{-1}) 1653 ($\nu_{C=O}$). ^{1}H NMR ($CDCl_3$, 500.13 MHz) δ 10.05 (s, 1H), 8.38−8.40 (m, 2H), 8.32 (s, 1H), 7.83−7.87 (m, 2H), 7.76 (s, 1H), 7.58−7.63 (m, 8H), 7.43−7.49 (m, 2H), 4.52 (m, 2H), 2.07 (m, 2H), 1.68 (s, 18H), 1.62 (m, 2H), 1.14−1.15 (m, 3H). ^{13}C NMR ($CDCl_3$, 125.77 MHz) δ 182.5, 147.4, 147.3, 142.9, 142.0, 141.5, 141.5, 139.7, 137.5, 137.4, 136.3, 134.9, 131.2, 129.1, 128.4, 127.3, 127.1, 126.2, 125.9, 124.3, 124.2, 124.0, 123.7, 123.4, 122.8, 121.4, 121.0, 118.4, 117.8, 116.3, 109.3, 107.3, 106.0, 43.1, 34.8, 32.1, 31.2, 20.6, 14.0. HRMS calcd for $C_{45}H_{45}N_2OS_2$ $[M+1]^+$ m/z 693.2967, found 693.2967.

(*E*)-3-(5-(9-Butyl-7-(9*H*-carbazol-9-yl)-9*H*-carbazol-2-yl)-thiophen-2-yl)-2-cyanoacrylic Acid (9a). It was prepared form **7a** (0.16 g, 0.33 mmol) and 2-cyano acetic acid (0.04 g, 0.5 mmol) by following a procedure described above for **5**. Red solid. Yield: 91%. (0.17 g); mp 214 °C. IR (KBr, cm^{-1}) 2216 ($\nu_{C\equiv N}$). ^{1}H NMR (DMSO-d_6, 500.13 MHz) δ 8.42 (d, J = 8.5 Hz, 1H), 8.29−8.32 (m, 3H), 8.25 (s, 1H), 8.07 (s, 1H), 7.92 (s, 1H), 7.86−7.88 (m, 2H), 7.62 (d, J = 7.0 Hz, 1H), 7.40−7.47 (m, 5H), 7.31−7.33 (m, 2H), 4.53 (m, 2H), 2.52 (m, 2H), 1.31−1.36 (m, 2H), 0.85−0.90 (m, 3H). ^{13}C NMR (DMSO-d_6, 125.77 MHz) δ 141.7, 141.2, 140.5, 137.0, 135.8, 135.0, 130.6, 126.2, 124.9, 122.7, 122.4, 121.9, 121.4, 121.0, 120.5, 120.0, 117.9, 117.7, 109.8, 108.0, 106.6, 42.1, 30.8, 19.7, 13.7. HRMS calcd for $C_{36}H_{28}N_3O_2S$ $[M+1]^+$ m/z 566.1896, found 566.1893.

(*E*)-3-(5-(5-(9-Butyl-7-(9*H*-carbazol-9-yl)-9*H*-carbazol-2-yl)-thiophen-2-yl)thiophen-2-yl)-2-cyanoacrylic Acid (10a). It was obtained in 92% (0.15 g) yield from **8a** (0.15 g, 0.25 mmol) by following a procedure similar to that described above for **5**. Red solid; mp 210 °C. IR (KBr, cm^{-1}) 2220 ($\nu_{C\equiv N}$). ^{1}H NMR (DMSO-d_6, 500.13 MHz) δ 8.51 (t, J = 12.0 Hz, 1H), 8.40 (q, J = 12.0 Hz, 1H), 8.25−8.31 (m, 3H), 7.97−8.06 (m, 2H), 7.90 (t, J = 11.5 Hz, 1H), 7.78−7.83 (m, 1H), 7.81 (dt, J = 12.0 Hz, 3.5 Hz, 1H), 7.59−7.67 (m, 2H), 7.37−7.51 (m, 5H), 7.27−7.35 (m, 2H), 4.52 (m, 2H), 1.77−1.80 (m, 2H), 1.33−1.37 (m, 2H), 0.87−0.92 (m, 2H). ^{13}C NMR (DMSO-d_6, 125.77 MHz) δ 163.6, 146.6, 146.3, 145.8, 141.6, 141.2, 140.6, 134.8, 133.80, 133.79, 130.65, 128.4, 126.2, 125.6, 124.8, 122.6, 122.0, 121.8, 121.3, 121.1, 120.5, 119.9, 117.8, 117.3, 116.6, 109.8, 108.0, 106.2, 42.1, 30.8, 19.8, 13.8. HRMS calcd for $C_{40}H_{29}N_3O_2S_2$ $[M]^+$ m/z 647.1695, found 647.1694.

(*E*)-3-(5-(9-Butyl-7-(3,6-di-*tert*-butyl-9*H*-carbazol-9-yl)-9*H*-carbazol-2-yl)thiophen-2-yl)-2-cyanoacrylic Acid (9b). It was synthesized in 89% (0.15 g) yield from **7b** (0.15 g, 0.25 mmol) by following a procedure similar to that described above for **5**. Orange solid; mp 224−226 °C. IR (KBr, cm^{-1}) 2219 ($\nu_{C\equiv N}$). ^{1}H NMR ($CDCl_3$, 500.13 MHz) δ 8.32 (s, 1H), 8.22 (d, J = 8.0 Hz, 1H), 8.19

(s, 2H), 8.12 (d, J = 8.0 Hz, 1.0 H), 7.79 (s, 1H), 7.71 (s, 1H), 7.59−7.61 (m, 2H), 7.55 (d, J = 3.0 Hz, 1H), 7.42−7.50 (m, 5H), 4.35 (m, 2H), 1.86−1.89 (m, 2H), 1.49 (s, 18H), 1.42−1.46 (m, 2H), 0.96 (t, J = 7.5 Hz, 3H). ^{13}C NMR ($CDCl_3$, 125.77 MHz) δ 157.5, 148.0, 142.9, 142.3, 141.4, 140.6, 139.5, 136.8, 134.5, 130.1, 124.7, 124.2, 123.7, 123.4, 121.7, 121.1, 118.5, 118.3, 116.3, 109.3, 107.3, 106.7, 43.2, 34.8, 32.1, 31.2, 20.6, 14.0. HRMS calcd for $C_{44}H_{43}N_3O_2S$ $[M]^+$ m/z 677.3070, found 677.3043.

(*E*)-3-(5-(5-(9-Butyl-7-(3,6-di-*tert*-butyl-9*H*-carbazol-9-yl)-9*H*-carbazol-2-yl)thiophen-2-yl)thiophen-2-yl)-2-cyanoacrylic Acid (10b). It was prepared in 86% (0.16 g) yield from **8b** (0.17 g, 0.25 mmol) by following a procedure similar to that described above for **5**. Red solid; mp 170 °C. IR (KBr, cm^{-1}) 2216 ($\nu_{C\equiv N}$); ^{1}H NMR (DMSO-d_6, 500.13 MHz) δ 8.32 (s, 1H), 8.22 (d, J = 8.0 Hz, 1H), 8.19 (s, 2H), 8.13 (d, J = 8.0 Hz, 1H), 7.79 (s, 1H), 7.71 (s, 1H), 7.60 (d, J = 9.0 Hz, 2H), 7.55 (d. J = 3.0 Hz, 1H), 7.42−7.50 (m, 5H), 4.33−4.34 (m, 2H), 1.88 (t, J = 7.5 Hz, 2H), 1.49 (s, 18H), 1.42−1.46 (m, 2H), 0.96 (t, J = 7.5 Hz, 3H). ^{13}C NMR (DMSO-d_6, 125.77 MHz) δ 172.0, 163.7, 146.6, 146.2, 145.7, 142.3, 141.6, 141.5, 141.2, 138.9, 135.3, 133.8, 133.8, 130.5, 128.3, 125.5, 124.8, 123.6, 122.7, 122.0, 121.7, 121.2, 120.7, 117.5, 117.3, 116.7, 116.6, 109.2, 107.5, 106.2, 98.0, 79.2, 42.1, 34.5, 31.8, 30.9, 19.8, 13.8. HRMS calcd for $C_{48}H_{45}N_3O_2S_2Na$ $[M+Na]^+$ m/z 782.2845, found 782.2825.

Computational Methods. Gaussian 09 program package[62] was used to perform all the computations. The ground-state geometries were fully optimized without any symmetry constraints using DFT employing a Becke's[63] hybrid correlation functional B3LYP[56] with 6-31g (d,p) basis set for all atoms. Vibrational analysis on the optimized structures was performed to confirm the structure. The excitation energies and oscillator strengths for the lowest 10 singlet−singlet transitions at the optimized geometry in the ground state were obtained by TD-DFT calculations using the same basis set with two different kinds of hybrid functionals namely B3LYP[56] and MPW1K.[57]

Crystal Structure Determination. Crystals of the compounds **7a** suitable for X-ray data collection were grown from dichloromethane/hexane mixture. X-ray data of was collected on a CCD diffractometer using Mo Kα (λ = 0.71073). The data were corrected for Lorentz and polarization effects. A total of 18 066 reflections were measured out of which 6153 were independent and 4133 were observed $[I > 2\sigma(I)]$ for maximum theta 27.47° at room temperature The structures were solved by direct methods using SHELXS-97[64] and refined by full-matrix least-squares refinement methods based on F^2, using SHELXL-97.[65] All non-hydrogen atoms were refined anisotropically. All hydrogen atoms were fixed geometrically with their U_{iso} values 1.2 times of the phenylene and methylene carbons and 1.5 times of the methyl carbons. All calculations were performed using WinGX package.[66] A final refinement of 335 parameters gave R_1 = 0.0448, wR_2 = 0.1200 for the observed data and R_1 = 0.0762, wR_2 = 0.1441 for all data.

Device Fabrication and Characterization. The TiO_2 colloid solution prepared from the TiO_2 precursor by sol−gel method as described below. Titanium(IV) tetraisopropoxide (72 mL) was added to 430 mL of a 0.1 M nitric acid aqueous solution with constant stirring and heated to 85 °C simultaneously for 8 h. After cooled the reaction mixture to room temperature, the resultant colloid was heated in an autoclave at 240 °C for 12 h to allow the TiO_2 particles to grow uniformly (ca. 20 nm). Consequently, the TiO_2 colloid was concentrated to 10 wt % (with respect to the TiO_2). The transparent layer was prepared by the addition 25 wt % (with respect to the TiO_2) PEG to the above solution to control the pore diameters to prevent the film from cracking during drying. The scattering layer prepared from the first type of TiO_2 paste incorporated with 50 wt % of light scattering TiO_2 particles (PT-501A, 15 $m^2 \cdot g^{-1}$, 100 nm, 99.74%) with respect to the 20 nm TiO_2 for reducing the light loss by back scattering.

A fluorine-doped SnO_2 conducting glass (FTO, 7 Ω sq^{-1}, transmittance ∼ 80%) was first cleaned with a neutral cleaner and then washed with deionized water, acetone, and isopropyl alcohol, sequentially. The conducting surface of the FTO was treated with a solution of titanium tetraisopropoxide (1.0 g) in 2-methoxyethanol (3.0 g) to obtain a good mechanical contact between the conducting glass and TiO_2 film, as well as to isolate the conducting glass surface from the electrolyte. TiO_2 pastes were coated on the conducting glass of FTO by doctor blade technique. For each coating TiO_2 layer, the dried TiO_2 film was gradually heated to 450 °C in an air flow and subsequently sintered at that temperature for 30 min. Finally FTO was coated with transparent layer (thickness 14.0 μm) and scattering layer (thickness 4.5 μm) of TiO_2 layer. After sintering at 450 °C cooled to 80 °C, the TiO_2 film was immersed in a 3×10^{-4} M dye bath at room temperature for 24 h. The absorption spectra of the dye loaded film measured with UV−visible spectrophotometer. The standard ruthenium complex, N719,[58] was dissolved in acetonitrile (ACN) and *tert*-butyl alcohol (volume ratio of 1:1) to make a reference dye solution. Various organic dye solutions were prepared in a mixing solvent containing ACN, *tert*-butanol and DMSO (volume ratio of 3.5:3.5:3). The hermetically cell prepared by connecting two electrodes by a hot melt 25 μm thick Surlyn film (SX1170-25) in which TiO_2/dye film as working electrode and platinum-sputtered conducting glass electrode (ITO, 7 Ω $sq.^{-1}$, transmittance > 80%) as counter electrode were used. The electrolyte consisting of 0.1 M LiI, 0.6 M DMPII, 0.05 M I_2, and 0.5 M TBP in 3-methoxypropionitrile (MPN)/ACN (volume ratio of 1:1) was introduced into the cell by capillary, and the hole was sealed with hot-melt glue after the injection of the electrolyte.

The irradiation source for the measurement of photocurrent−voltage is a class-A quality solar simulator (XES-301S, AM1.5G) with incident intensity (100 mW cm^{-2}) and the surface of the DSSC covered by a mask with a light-illuminated area of 0.16 cm^2. The light intensity was calibrated with a standard Si cell (PECSI01). Photoelectrochemical characteristics of the DSSCs were obtained with a potentiostat/galvanostat. For the electrochemical impedance spectra (EIS), potentiostat/galvanostat equipped with an FRA2 module, under a constant light illumination of 100 mW cm^{-2}, and the range of frequency applied was 10 mHz to 65 kHz. The impedance spectra were analyzed using an equivalent circuit model. Incident photon-to-current conversion efficiency (IPCE) curves were obtained at short-circuit condition. The light source was a class-A quality solar simulator (PEC-L11, AM 1.5 G); light was focused through a monochromator onto the photovoltaic cell. The monochromator was incremented through the visible spectrum to generate the IPCE (λ) as defined by IPCE (λ) = 1240 ($J_{SC}/\lambda\varphi$), where λ is the wavelength, J_{SC} is short-circuit photocurrent (mA cm^{-2}) recorded with a potentiostat/galvanostat, and φ is the incident radiative flux (W m^{-2}) measured with an optical detector and power meter.

■ ASSOCIATED CONTENT

Ⓢ Supporting Information

Copies of ^{1}H NMR and ^{13}C NMR spectra absorption spectra of the dyes recorded in different solvents, absorption data in different solvents, electrochemical data for the dyes in acetonitrile, Cartesian coordinates for the optimized structures, and TDDFT computations results. This material is available free of charge via the Internet at http://pubs.acs.org.

■ AUTHOR INFORMATION

Corresponding Author

*E-mail: krjt8fcy@iitr.ernet.in. Phone: +91-1332-285376.

Notes

The authors declare no competing financial interest.

■ ACKNOWLEDGMENTS

K.R.J.T. is thankful to Department of Science and Technology, New Delhi, India for financial support (Ref. No. DST/TSG/PT/2013/09). A.V. acknowledges a senior research fellowship from UGC, New Delhi.

REFERENCES

(1) Ahmad, S.; Guillén, E.; Kavan, L.; Grätzel, M.; Nazeeruddin, M. K. Metal Free Sensitizer and Catalyst for Dye Sensitized Solar Cells. *Energy Environ. Sci.* **2013**, *6*, 3439−3466.

(2) Zhang, Q. G.; Dandeneau, C. S.; Zhou, X.-Y.; Cao, G.-Z. ZnO Nanostructures for Dye-Sensitized Solar Cells. *Adv. Mater.* **2009**, *21*, 4087−4108.

(3) Wu, Y.-Z.; Zhu, W.-H. Organic Sensitizers from D-π-A to D-A-π-A: Effect of the Internal Electron-Withdrawing Units on Molecular Absorption, Energy Levels and Photovoltaic Performances. *Chem. Soc. Rev.* **2013**, *42*, 2039−2058.

(4) Haid, S.; Marszalek, M.; Mishra, A.; Wielopolski, M.; Joël, T.; Moser, J.-E.; Humphry-Baker, R.; Zakeeruddin, S. M.; Grätzel, M.; Bäuerle, P. Significant Improvement of Dye-Sensitized Solar Cell Performance by Small Structural Modification in π-Conjugated Donor-Acceptor Dyes. *Adv. Funct. Mater.* **2012**, *22*, 1291−1302.

(5) Yen, Y.-S.; Chou, H.-H.; Chen, Y.-C.; Hsu, C.-Y.; Lin, J. T. Recent Developments in Molecule-Based Organic Materials for Dye-Sensitized Solar Cells. *J. Mater. Chem.* **2012**, *22*, 8734−8747.

(6) Kim, B.-G.; Chung, K.; Kim, J. Molecular Design Principle of All-Organic Dyes for Dye-Sensitized Solar Cells. *Chem.—Eur. J.* **2013**, *19*, 5220−5230.

(7) Mishra, A.; Fischer, M. K. R.; Bäuerle, P. Metal-Free Organic Dyes for Dye-Sensitized Solar Cells: From Structure: Property Relationships to Design Rules. *Angew. Chem., Int. Ed.* **2009**, *48*, 2474−2499.

(8) Ooyama, Y.; Harima, Y. Photophysical and Electrochemical Properties, and Molecular Structures of Organic Dyes for Dye-Sensitized Solar Cells. *ChemPhysChem* **2012**, *13*, 4032−4080.

(9) Liang, M.; Chen, J. Arylamine Organic Dyes for Dye-Sensitized Solar Cells. *Chem. Soc. Rev.* **2013**, *42*, 3453−3488.

(10) Hagfeldt, A.; Boschloo, G.; Sun, L.; Kloo, L.; Pettersson, H. Dye-Sensitized Solar Cells. *Chem. Rev.* **2010**, *110*, 6595−6663.

(11) Barea, E. M.; Bisquert, J. Properties of Chromophores Determining Recombination at the TiO_2-Dye-Electrolyte Interface. *Langmuir* **2013**, *29*, 8773−8781.

(12) Cui, Y.; Wu, Y.; Lu, X.; Zhang, X.; Zhou, G.; Miapeh, F. B.; Zhu, W.; Wang, Z.-S. Incorporating Benzotriazole Moiety to Construct D-A-π-A Organic Sensitizers for Solar Cells: Significant Enhancement of Open-Circuit Photovoltage with Long Alkyl Group. *Chem. Mater.* **2011**, *23*, 4394−4401.

(13) Koumura, N.; Wang, Z.-S.; Mori, S.; Miyashita, M.; Suzuki, E.; Hara, K. Alkyl-Functionalized Organic Dyes for Efficient Molecular Photovoltaics. *J. Am. Chem. Soc.* **2006**, *128*, 14256−14257.

(14) Wang, Z.-S.; Koumura, N.; Cui, Y.; Takahashi, M.; Sekiguchi, H.; Mori, A.; Kubo, T.; Furube, A.; Hara, K. Hexylthiophene-Functionalized Carbazole Dyes for Efficient Molecular Photovoltaics: Tuning of Solar-Cell Performance by Structural Modification. *Chem. Mater.* **2008**, *20*, 3993−4003.

(15) Hu, X.; Cai, S.; Tian, G.; Li, X.; Su, J.; Li, J. Rigid Triarylamine-Based D-A-π-A Structural Organic Sensitizers for Solar Cells: The Significant Enhancement of Open-Circuit Photovoltage with a Long Alkyl Group. *RSC Adv.* **2013**, *3*, 22544−22553.

(16) Ren, X.; Jiang, S.; Cha, M.; Zhou, G.; Wang, Z.-S. Thiophene-Bridged Double D-π-A Dye for Efficient Dye-Sensitized Solar Cell. *Chem. Mater.* **2012**, *24*, 3493−3499.

(17) Cao, D.; Peng, J.; Hong, Y.; Fang, X.; Wang, L.; Meier, H. Enhanced Performance of the Dye-Sensitized Solar Cells with Phenothiazine-Based Dyes Containing Double D-A Branches. *Org. Lett.* **2011**, *13*, 1610−1613.

(18) Baheti, A.; Thomas, K. R. J.; Lee, C.-P.; Ho, K.-C. Synthesis and Characterization of Dianchoring Organic Dyes Containing 2,7-Diaminofluorene Donors as Efficient Sensitizers for Dye-Sensitized Solar Cells. *Org. Electron.* **2013**, *14*, 3267−3276.

(19) Kotchapradist, P.; Prachumrak, N.; Tarsang, R.; Jungsuttiwong, S.; Keawin, T.; Sudyoadsuk, T.; Promarak, V. Pyrene-Functionalized Carbazole Derivatives as Non-Doped Blue Emitters for Highly Efficient Blue Organic Light-Emitting Diodes. *J. Mater. Chem. C* **2013**, *1*, 4916−4924.

(20) Cui, L.-S.; Dong, S.-C.; Liu, Y.; Li, Q.; Jiang, Z.-Q.; Liao, L.-Z. A Simple Systematic Design of Phenylcarbazole Derivatives for Host Materials to High-Efficiency Phosphorescent Organic Light-Emitting Diodes. *J. Mater. Chem. C* **2013**, *1*, 3967−3975.

(21) Thomas, K. R. J.; Lin, J. T.; Tao, Y.-T.; Ko, C.-W. Light-Emitting Carbazole Derivatives: Potential Electroluminescent Materials. *J. Am. Chem. Soc.* **2001**, *123*, 9404−9411.

(22) Ooyama, Y.; Inoue, S.; Nagano, T.; Kushimoto, K.; Ohshita, J.; Imae, I.; Komaguchi, K.; Harima, Y. Dye-Sensitized Solar Cells Based On Donor-Acceptor π-Conjugated Fluorescent Dyes with a Pyridine Ring as an Electron-Withdrawing Anchoring Group. *Angew. Chem., Int. Ed.* **2011**, *50*, 7429−7433.

(23) Ooyama, Y.; Nagano, T.; Inoue, S.; Imae, I.; Komaguchi, K.; Ohshita, J.; Harima, Y. Dye-Sensitized Solar Cells Based on Donor-π-Acceptor Fluorescent Dyes with a Pyridine Ring as an Electron-Withdrawing-Injecting Anchoring Group. *Chem.—Eur. J.* **2011**, *17*, 14837−14843.

(24) Venkateswararao, A.; Thomas, K. R. J.; Lee, C.-P.; Ho, K.-C. Synthesis and Characterization of Organic Dyes Containing 2,7-Disubstituted Carbazole π-Linker. *Tetrahedron Lett.* **2013**, *54*, 3985−3989.

(25) Venkateswararao, A., Thomas, K. R. J. In *Solar Cell Nanotechnology*; Tiwari, A., Boukherroub, R., Sharon, M., Eds.; Wiley-Scrivener: Beverly, MA, 2014; Chapter 2, pp 41−96.

(26) Wang, H.-Y.; Liu, F.; Xie, L.-H.; Tang, C.; Peng, B.; Huang, W.; Wei, W. Topological Arrangement of Fluorenyl-Substituted Carbazole Triads and Starbursts: Synthesis and Optoelectronic Properties. *J. Phys. Chem. C* **2011**, *115*, 6961−6967.

(27) Huang, H.; Fu, Q.; Pan, B.; Zhuang, S.; Wang, L.; Chen, J.; Ma, D.; Yang, C. Butterfly-Shaped Tetrasubstituted Carbazole Derivatives as a New Class of Hosts for Highly Efficient SolutionProcessable Green Phosphorescent Organic Light-Emitting Diodes. *Org. Lett.* **2012**, *14*, 4786−4789.

(28) Brunner, K.; van Dijken, A.; Börner, H.; Bastiaansen, J. J. A. M.; Kiggen, N. M. M.; Langeveld, B. M. W. Carbazole Compounds as Host Materials for Triplet Emitters in Organic Light-Emitting Diodes: Tuning the HOMO Level without Influencing the Triplet Energy in Small Molecules. *J. Am. Chem. Soc.* **2004**, *126*, 6035−6042.

(29) Teng, C.; Yang, X.; Li, S.; Cheng, M.; Hagfeldt, A.; Wu, L.; Sun, L. Tuning the HOMO Energy Levels of Organic Dyes for Dye-Sensitized Solar Cells Based on Br^-/Br_3^- Electrolytes. *Chem.—Eur. J.* **2010**, *16*, 13127−13138.

(30) Lee, W.; Cho, N.; Kwon, J.; Ko, J.; Hong, J.-I. New Organic Dye Based on a 3,6-Disubstituted Carbazole Donor for Efficient Dye-Sensitized Solar Cells. *Chem.—Asian J.* **2012**, *7*, 343−350.

(31) Sudyoadsuk, T.; Pansay, S.; Morada, S.; Rattanawan, R.; Namuangruk, S.; Kaewin, T.; Jungsuttiwong, S.; Promarak, V. Synthesis and Characterization of D-D-π-A-Type Organic Dyes Bearing Carbazole-Carbazole as a Donor Moiety (D-D) for Efficient Dye-Sensitized Solar Cells. *Eur. J. Org. Chem.* **2013**, 5051−5063.

(32) Yella, A.; Humphry-Baker, R.; Curchod, B. F. E.; Astani, N. S.; Teuscher, J.; Polander, L. E.; Mathew, S.; Moser, J.-E.; Tavernelli, I.; Rothlisherger, U.; Grätzel, M.; Nazeeruddin, M. K.; Frey, J. Molecular Engineering of a Fluorene Donor for Dye-Sensitized Solar Cells. *Chem. Mater.* **2013**, *25*, 2733−2739.

(33) Monnier, F.; Taillefer, M. Catalytic C-C, C-N, and C-O Ullmann-Type Coupling Reactions. *Angew. Chem., Int. Ed.* **2009**, *48*, 6954−6971.

(34) Liu, Y.; Nishiura, M.; Wang, Y.; Hou, Z. π-Conjugated Aromatic Enynes as a Single-Emitting Component for White Electroluminescence. *J. Am. Chem. Soc.* **2006**, *128*, 5592−5593.

(35) Freeman, A. W.; Urvoy, M.; Criswell, M. E. Triphenylphosphine-Mediated Reductive Cyclization of 2-Nitrobiphenyls: A Practical and Convenient Synthesis of Carbazoles. *J. Org. Chem.* **2005**, *70*, 5014−5019.

(36) Che, Y.; Gross, D. E.; Huang, H.; Yang, D.; Yang, X.; Discekici, E.; Xue, Z.; Zhao, H.; Moore, J. S.; Zang, L. Diffusion-Controlled Detection of Trinitrotoluene: Interior Nanoporous Structure and Low

Highest Occupied Molecular Orbital Level of Building Blocks Enhance Selectivity and Sensitivity. *J. Am. Chem. Soc.* **2012**, *134*, 4978−4982.
(37) Stille, J. K. The Palladium-Catalyzed Cross-Coupling Reactions of Organotin Reagents with Organic Electrophiles. *Angew. Chem., Int. Ed.* **1986**, *25*, 508−524.
(38) Knoevenagel, E. Ueber eine Darstellungsweise des Benzylidenacetessigesters. *Chem. Ber.* **1896**, *29*, 172−174.
(39) Zhu, W.; Wu, Y.; Wang, S.; Li, W.; Li, X.; Chen, J.; Wang, Z.-S.; Tian, H. Organic D-A-π-A Solar Cell Sensitizers with Improved Stability and Spectral Response. *Adv. Funct. Mater.* **2011**, *21*, 756−763.
(40) Kim, J.-J.; Choi, H.; Lee, J.-W.; Kang, M.-S.; Song, K.; Kang, S. O.; Ko, J. A Polymer Gel Electrolyte to Achieve ≥ 6% Power Conversion Efficiency with a Novel Organic Dye Incorporating a Low-Band-Gap Chromophore. *J. Mater. Chem.* **2008**, *18*, 5223−5229.
(41) Thomas, K. R. J.; Hsu, Y.-C.; Lin, J. T.; Lee, K.-M.; Ho, K.-C.; Lai, C.-H.; Cheng, Y.-M.; Chou, P.-T. 2,3-Disubstituted Thiophene-Based Organic Dyes for Solar Cells. *Chem. Mater.* **2008**, *20*, 1830−1840.
(42) Mishra, A.; Pootrakulchote, N.; Wang, M.; Moon, S.-J.; Zakeeruddin, S. M.; Grätzel, M.; Bäuerle, P. A Thiophene-Based Anchoring Ligand and Its Heteroleptic Ru(II)-Complex for Efficient Thin-Film Dye-Sensitized Solar Cells. *Adv. Funct. Mater.* **2011**, *21*, 963−970.
(43) Barea, E. M.; Zafer, C.; Gultekin, B.; Aydin, B.; Koyuncu, S.; Icli, S.; Santiago, F. F.; Bisquert, J. Quantification of the Effects of Recombination and Injection in the Performance of Dye-Sensitized Solar Cells Based on *N*-Substituted Carbazole Dyes. *J. Phys. Chem. C* **2010**, *114*, 19840−19848.
(44) Nazeeruddin, M. K.; Péchy, P.; Renouard, T.; Zakeeruddin, S. M.; Humphry-Baker, R.; Comte, P.; Liska, P.; Cevey, L.; Costa, E.; Shklover, V.; Spiccia, L.; Deacon, G. B.; Bignozzi, C. A.; Grätzel, M. Engineering of Efficient Panchromatic Sensitizers for Nanocrystalline TiO_2-Based Solar Cells. *J. Am. Chem. Soc.* **2001**, *123*, 1613−1624.
(45) Nazeeruddin, M. K.; Zakeeruddin, S. M.; Humphry-Baker, R.; Jirousek, M.; Liska, P.; Vlachopoulos, N.; hklover, V.; Fisher, C. H.; Grätzel, M. Acid-Base Equilibria of (2,2′-Bipyridyl-4,4′-dicarboxylic acid)ruthenium(II) Complexes and the Effect of Protonation on Charge-Transfer Sensitization of Nanocrystalline Titania. *Inorg. Chem.* **1999**, *38*, 6298−6305.
(46) Wang, Z.-S.; Li, F.-Y.; Huang, C.-H. Photocurrent Enhancement of Hemicyanine Dyes Containing RSO_3-Group through Treating TiO_2 Films with Hydrochloric Acid. *J. Phys. Chem. B* **2001**, *105*, 9210−9217.
(47) Singh, P.; Baheti, A.; Thomas, K. R. J. Synthesis and Optical Properties of Acidochromic Amine-Substituted Benzo[*a*]phenazines. *J. Org. Chem.* **2011**, *76*, 6134−6145.
(48) Baheti, A.; Tyagi, P.; Thomas, K. R. J.; Hsu, Y.-C.; Lin, J. T. Simple Triarylamine-Based Dyes Containing Fluorene and Biphenyl Linkers for Efficient Dye-Sensitized Solar Cells. *J. Phys. Chem. Lett.* **2009**, *113*, 8541−8547.
(49) van den Berg, O.; Jager, W. F.; Picken, S. J. 7-Dialkylamino-1-alkylquinolinium Salts: Highly Versatile and Stable Fluorescent Probes. *J. Org. Chem.* **2006**, *71*, 2666−2676.
(50) Granzhan, A.; Ihmels, H.; Viola, G. 9-Donor-Substituted Acridizinium Salts: Versatile Environment-Sensitive Fluorophores for the Detection of Biomacromolecules. *J. Am. Chem. Soc.* **2007**, *129*, 1254−1267.
(51) Sayama, K.; Tsukagoshi, S.; Hara, K.; Ohga, Y.; Shinpou, A.; Abe, Y.; Suga, S.; Arakawa, H. Photoelectrochemical Properties of J Aggregates of Benzothiazole Merocyanine Dyes on a Nanostructured TiO_2 Film. *J. Phys. Chem. B* **2002**, *106*, 1363−1371.
(52) Teng, C.; Yang, X.; Yang, C.; Tian, H.; Li, S.; Wang, X.; Hagfeldt, A.; Sun, L. Influence of Triple Bonds as π-Spacer Units in Metal-Free Organic Dyes for Dye-Sensitized Solar Cells. *J. Phys. Chem. C* **2010**, *114*, 11305−11313.
(53) Morin, J.-F.; Leclerc, M.; Adès, D.; Siove, A. Polycarbazoles: 25 Years of Progress. *Macromol. Rapid Commun.* **2005**, *26*, 761−778.
(54) Kato, S.; Noguchi, H.; Kobayashi, A.; Yoshihara, T.; Tobita, S.; Nakamura, Y. Bicarbazoles: Systematic Structure-Property Investigations on a Series of Conjugated Carbazole Dimers. *J. Org. Chem.* **2012**, *77*, 9120−9133.
(55) Grätzel, M. Photoelectrochemical cells. *Nature* **2001**, *414*, 338−344.
(56) Parr, R. G.; Yang, W. Density-Functional Theory of the Electronic Structure of Molecules. *Annu. Rev. Phys. Chem.* **1995**, *46*, 701−728.
(57) Lynch, B. J.; Fast, P. L.; Harris, M.; Truhlar, D. G. Adiabatic Connection for Kinetics. *J. Phys. Chem. A* **2000**, *104*, 4811−4815.
(58) Nazeeruddin, M. K.; Kay, A.; Rodicio, I.; Humphry-Baker, R.; Müller, E.; Liska, P.; Vlachopoulos, N.; Grätzel, M. Conversion of Light to Electricity by cis-X2bis(2,2′-bipyridyl-4,4′-dicarboxylate)-ruthenium(II) Charge-Transfer Sensitizers (X = Cl-, Br-, I-, CN-, and SCN-) on Nanocrystalline Titanium Dioxide Electrodes. *J. Am. Chem. Soc.* **1993**, *115*, 6382−6390.
(59) Raga, S. R.; Barea, E. M.; Fabregat-Santiago, F. Analysis of the Origin of Open Circuit Voltage in Dye Solar Cells. *J. Phys. Chem. Lett.* **2012**, *3*, 1629−1634.
(60) Li, G.; Liang, M.; Wang, H.; Sun, Z.; Wang, L.; Wang, Z.; Xue, S. Significant Enhancement of Open-Circuit Voltage in Indoline-Based Dye-Sensitized Solar Cells via Retarding Charge Recombination. *Chem. Mater.* **2013**, *25*, 1713−1722.
(61) Haque, S. A.; Tachibana, Y.; Willis, R. L.; Moser, J. E.; Grätzel, M.; Klug, D. R.; Durrant, J. R. Parameters Influencing Charge Recombination Kinetics in Dye-Sensitized Nanocrystalline Titanium Dioxide Films. *J. Phys. Chem. B* **2000**, *104*, 538−547.
(62) Frisch, M. J.; Trucks, G. W.; Schlegel, H. B.; Scuseria, G. E.; Robb, M. A.; Cheeseman, J. R.; Scalmani, G.; Barone, V.; Mennucci, B.; Petersson, G. A.; Nakatsuji, H.; Caricato, M.; Li, X.; Hratchian, H. P.; Izmaylov, A. F.; Bloino, J.; Zheng, G.; Sonnenberg, J. L.; Hada, M.; Ehara, M.; Toyota, K.; Fukuda, R.; Hasegawa, J.; Ishida, M.; Nakajima, T.; Honda, Y.; Kitao, O.; Nakai, H.; Vreven, T.; Montgomery, J. A.; Peralta, J. E.; Ogliaro, F.; Bearpark, M.; Heyd, J. J.; Brothers, E.; Kudin, K. N.; Staroverov, V. N.; Kobayashi, R.; Normand, J.; Raghavachari, K.; Rendell, A.; Burant, J. C.; Iyengar, S. S.; Tomasi, J.; Cossi, M.; Rega, N.; Millam, N. J.; Klene, M.; Knox, J. E.; Cross, J. B.; Bakken, V.; Adamo, C.; Jaramillo, J.; Gomperts, R.; Stratmann, R. E.; Yazyev, O.; Austin, A. J.; Cammi, R.; Pomelli, C.; Ochterski, J. W.; Martin, R. L.; Morokuma, K.; Zakrzewski, V. G.; Voth, G. A.; Salvador, P.; Dannenberg, J. J.; Dapprich, S.; Daniels, A. D.; Farkas, O.; Foresman, J. B.; Ortiz, J. V.; Cioslowski, J.; Fox, D. J. *Gaussian 09*, Revision A.02; Gaussian, Inc.: Wallingford, CT, 2009.
(63) Becke, A. D. A New Mixing of Hartree-Fock and Local Density-Functional Theories. *J. Chem. Phys.* **1993**, *98*, 1372−1377.
(64) Sheldrick, G. M. *SHELXS-97: Program for Crystal Structure Determination*; University of Göttingen: Germany, 1997.
(65) Sheldrick, G. M. *SHELXL-97: Program for the Refinement of Crystal Structure*; University of Göttingen: Germany, 1997.
(66) Farrugia, L. J. WinGX and ORTEP for Windows: an Update. *J. Appl. Crystallogr.* **2012**, *45*, 849−854.